ADVANCED BIOSYSTEMS
www.adv-biosys.com

Bioinspired Precision Engineering of Three-Dimensional Epithelial Stem Cell Microniches

*Elisabetta Prina, Mahetab H. Amer, Laura Sidney, Maximilian Tromayer, Jonathan Moore, Robert Liska, Marina Bertolin, Stefano Ferrari, Andrew Hopkinson, Harminder Dua, Jing Yang, Ricky Wildman, and Felicity R. A. J. Rose**

Maintenance of the epithelium relies on stem cells residing within specialized microenvironments, known as epithelial crypts. Two-photon polymerization (2PP) is a valuable tool for fabricating 3D micro/nanostructures for stem cell niche engineering applications. Herein, biomimetic gelatin methacrylate-based constructs, replicating the precise geometry of the limbal epithelial crypt structures (limbal stem cell "microniches") as an exemplar epithelial niche, are fabricated using 2PP. Human limbal epithelial stem cells (hLESCs) are seeded within the microniches in xeno-free conditions to investigate their ability to repopulate the crypts and the expression of various differentiation markers. Cell proliferation and a zonation in cell phenotype along the *z*-axis are observed without the use of exogenous signaling molecules. Significant differences in cell phenotype between cells located at the base of the microniche and those situated towards the rim are observed, demonstrating that stem cell fate is strongly influenced by its location within a niche and the geometrical details of where it resides. This study provides insight into the influence of the niche's spatial geometry on hLESCs and demonstrates a flexible approach for the fabrication of biomimetic crypt-like structures in epithelial tissues. This has significant implications for regenerative medicine applications and can ultimately lead to implantable synthetic "niche-based" treatments.

In the body, stem cells are located in complex microenvironments, called niches, where they can reside indefinitely, self-renew, and produce progeny cells.[1] By grouping stem cells into microniches, tissues have control over maintenance and regeneration.[2] This is tightly regulated by intrinsic and extrinsic factors, such as nuclear factors[3] and cues from the surrounding microenvironment.[4,5] The microenvironment offers cues that regulate cell behavior, including proliferation and differentiation. A crucial aspect to control stem cell fate for regenerative medicine-based therapies is being able to reproduce this instructive microenvironment, or "microniche." Advancing stem cell niche engineering is particularly important for regenerative medicine applications, including the development of predictive disease models, stem cell therapies, and tissue-engineered constructs.

Current research into supporting epithelial regeneration has focused on studying the effects of extracellular matrix (ECM) composition, cell–cell interactions, and influences of surface chemistry and topography.[6,7] The impact of geometrical cues and their role in the regulation of the niche have not been fully explored. Moreover, epithelial stem cell therapies have largely ignored the niche and focused on cell populations to be transplanted, and this neglect leads to a lack of control over stem cell behavior that may contribute to the high failure rates of cell therapies.[8–10] In addition to mechanical cues,

Dr. E. Prina, Dr. M. H. Amer, Dr. J. Yang, Prof. F. R. A. J. Rose
Division of Regenerative Medicine and Cellular Therapies
School of Pharmacy
Nottingham Biodiscovery Institute
University of Nottingham
Nottingham NG7 2RD, UK
E-mail: felicity.rose@nottingham.ac.uk

Dr. L. Sidney, Dr. A. Hopkinson, Prof. H. Dua
Academic Ophthalmology
Division of Clinical Neuroscience
University of Nottingham
Nottingham NG7 2UH, UK

The ORCID identification number(s) for the author(s) of this article can be found under https://doi.org/10.1002/adbi.202000016.

DOI: 10.1002/adbi.202000016

Dr. M. Tromayer, Prof. R. Liska
Institute of Applied Synthetic Chemistry
Vienna University of Technology
Getreidemarkt 9/163, Vienna 1060, Austria

Dr. J. Moore
School of Chemistry
University of Nottingham
Nottingham NG7 2RD, UK

Dr. M. Bertolin, Dr. S. Ferrari
Fondazione Banca degli Occhi del Veneto Onlus
Padiglione Rama
Via Paccagnella 11, Zelarino-Venezia 30174, Italy

Prof. R. Wildman
Institute of Advanced Manufacturing
Faculty of Engineering
University of Nottingham
Nottingham NG7 2RD, UK

we hypothesized that spatial geometry plays a crucial role in determining stem cell fate. Our aim was to recreate the precise geometry of an epithelial stem cell niche using two-photon polymerization (2PP) and to determine the role of spatial geometry on stem cell phenotype in a 3D microniche setting.

Geometrical cues have been reported to influence gene expression on 2D micropatterned substrates,[11–14] but little is known about how geometrical cues influence cell behavior in 3D "niche-like" settings. In this study, the influence of spatial geometry on the differentiation of stem cells was investigated, independent of imposed chemical and environmental conditions. As an exemplar, we focused on the limbal stem cell niche. The limbus is the niche responsible for long-term renewal of the cornea.[15] It is a 1 mm-wide circular region separating the sclera from the cornea. It contains the palisades of Vogt,[16,17] some of which are associated with limbal epithelial crypts (LECs). Three types of stem cell niches have been identified in the limbal region: LECs, limbal crypts, and focal stromal projections.[18] The presence, location, and shape of LECs were described for the first time by Dua et al.[19,20] During healing and homeostasis, human limbal epithelial stem cells (hLESCs), also known as corneal epithelial stem cells, migrate towards the center of the cornea and differentiate[21] to constantly replace corneal epithelial cells.[22] Such niche structures are common in all epithelial tissues and share certain characteristics, including geometry, a stromal compartment, and zonation in epithelial cell phenotype. This zonation is such that there is a stem cell zone, a progenitor (transiently amplifying) cell zone, and a region where cells are terminally differentiated.[23]

We used 2PP to create gelatin-based 3D crypts that mimic the precise geometry of the limbal stem cell niche. 2PP is an additive manufacturing technique capable of fabricating 3D micro/nanostructures without a mask and with a possible feature size of <100 nm. This is achieved through the absorption of multiple photons simultaneously, usually in the infrared range, and the requirements for such an event result in small region of illumination with a sufficient intensity of photons to initiate polymerization.[24]

Using histological sections described by Dua et al.,[19] crypt dimensions were identified and a 3D tapered geometry was designed to replicate the niche using computer-aided design (CAD) software (**Figure 1**). These structures were then fabricated by 2PP from gelatin methacrylate (GelMA) as concave scaffolds, with a 200 µm opening tapering to a 20 µm point at the base. GelMA is being increasingly used in tissue engineering due to its biocompatibility and tunable physicochemical properties, enabling control over the mechanical properties of the gel.[25] GelMA presented a degree of methacrylation of 80.2% ± 6.1%, confirmed by the trinitrobenzenesulfonic acid (TNBS) assay (Figure S1, Supporting Information). The microniche constructs were successfully printed and they closely replicated the CAD model (Figure 1).

Following the creation of the niche-mimicking geometries, hLESCs (commercial hLESCs and biopsy-derived td_hLESCs) were seeded inside the niches in xeno-free conditions to

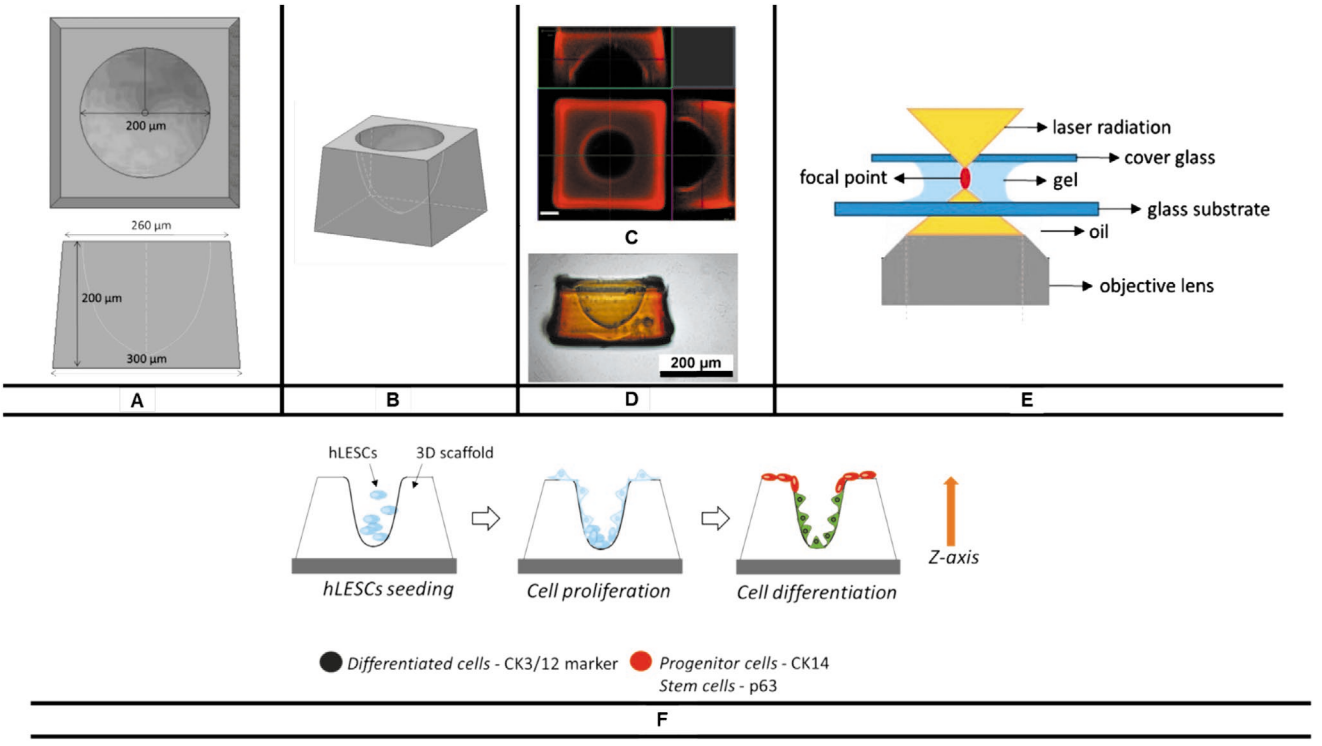

Figure 1. Limbal stem cell niche fabrication and assessment of cell response. A) Top and side views and B) 3D reconstruction of the CAD model developed to mimic the in vivo structure. C) Confocal images of top and side views of the printed structure (scale bar = 50 µm). D) Brightfield image of the side view of the printed niche. E) Configuration of gel setup and 2PP system, where the gel is sandwiched between two cover glasses and the laser is focused with 25× or 63× objectives. F) Graphical representation of cell experiments: hLESCs are seeded on the microniches; proliferation is monitored and differentiation assessed.

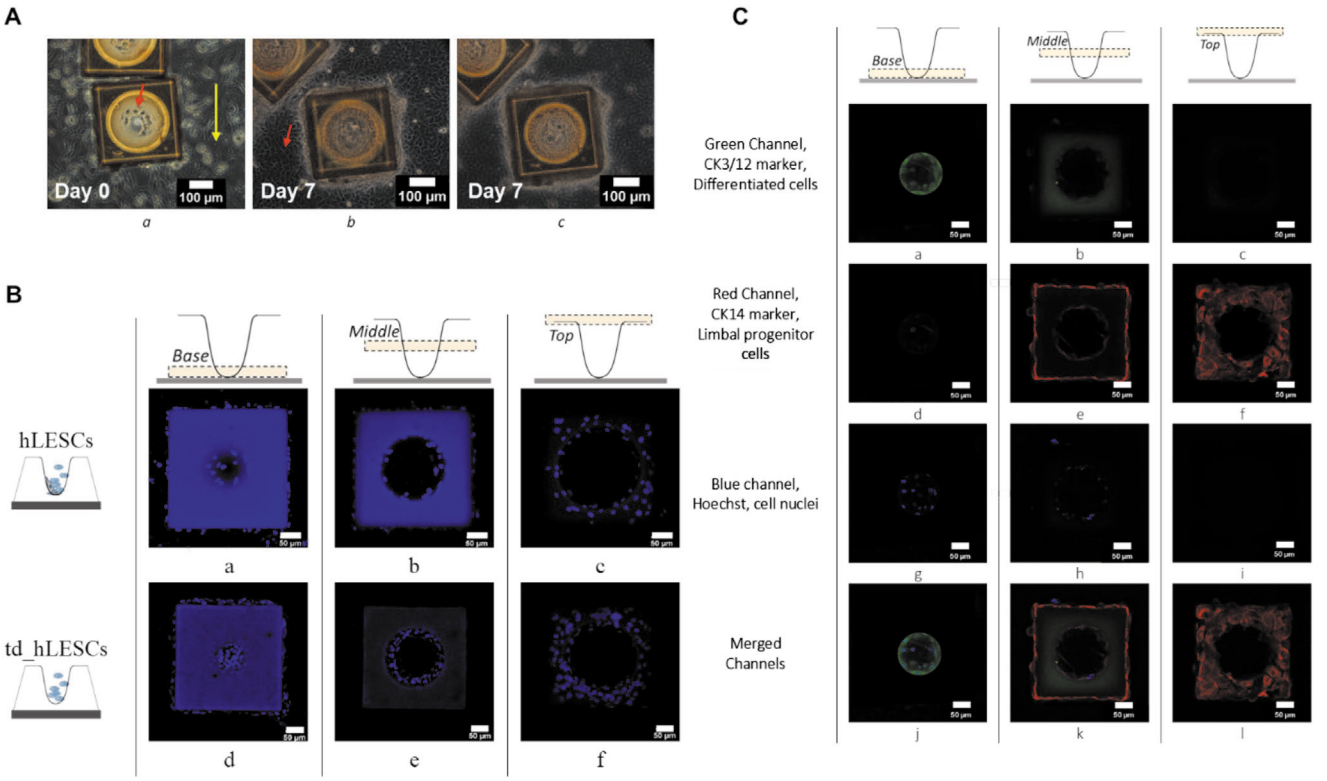

Figure 2. Proliferation and zonation of marker expression. A) Limbal epithelial stem cells (td_hLESCs) immediately a) after seeding and after b,c) 7 days in culture. The focus is on the b) top and c) bottom of the microniche structure. The yellow arrow indicates the feeder layer, and the red arrow indicates keratinocytes presenting a polygonal morphology. B) Distribution of primary cells along the *z*-axis, shown by *z*-stack confocal images of cells at the base, middle, and top of the structure. Commercially available a–c) hLESCs or d–f) a feeder layer of irradiated 3T3-J2 cells+td_hLESCs were seeded, and distribution along the microniche was monitored using Hoechst 33258. C) Three *z*-positions representing a,d,g) the base, b,e,h) the middle, and c,f,i) rim of the microniche. For the base, the area surrounding the center has been darkened to highlight the structure's base. hLESCs were stained with CK3/12 (green; differentiated cells), CK14 (red; limbal progenitor cells), and Hoechst (blue; nuclei). a–c) Green, d–f) red, g–i) blue, and j–l) merged channels are presented. The majority of the cells on the base expressed the differentiation marker CK 3/12 (green), while the majority at the rim expressed the progenitor cell marker CK14 (red). Images are representative of three independent experiments.

investigate their ability to repopulate the crypts and to study their differentiation. hLESCs (CELLnTEC; Switzerland) presented a homogenous monolayer of single cells (Figure S2, Supporting Information). Td_hLESCs were seeded on an irradiated 3T3-feeder layer, and these feeder cells were later removed by changing the media upon keratinocyte confluency (Figure S2, Supporting Information), leaving the cells of interest on the scaffold. After seeding, cells proliferated and were distributed along the length of the concave crypt, from the base to the rim (**Figure 2**A,B). Cell differentiation was studied along the *z*-axis, using cytokeratin 14 (CK14) and cytokeratin 3/12 (CK3/12) as markers for limbal progenitor cells and differentiated corneal epithelial cells, respectively.[26,27] Zonation in marker expression was observed along the *z*-axis, presenting differentiated cells on the base (CK3/12; green) and limbal progenitor cells (CK14; red) at the rim (Figure 2C; Figure S3, Supporting Information). As CK14 is a progenitor cell marker (rather than a stem cell marker, such as p63), we conclude that cells expressing this marker represent a cell population at an early stage of the differentiation pathway.

Atomic force microscopy (AFM) was conducted to identify the stiffness of the synthetic microniche, as it allows elastic modulus measurements to be performed at the same length scales at which cells interact with material.[28] Due to the length of the AFM tip, the base of the scaffold was not accessible; hence, its properties could not be measured. Therefore, the base was measured using a flat structure fabricated with the same printing parameters used for making the base of the concave microniche (**Figure 3**A). Results indicated that there was a notable difference between the mean values of elastic moduli in the *z*-direction with the top always stiffer than the base (75.60 vs 25.87, 92.39 vs 16.05, and 25.11 vs 5.46 kPa). However, the inherent variability associated with AFM measurements resulted in statistical nonsignificance ($p = 0.09$, $n = 3$). Elastic moduli were in the same order of magnitude of the cornea, which was also assessed by AFM (7.5–110 kPa[29]). This range of values describes the local stiffness variations occurring in the transition from the limbal to the surface of the cornea.[30,31] To our knowledge, there are no studies so far that have shown correlation between stiffness and *z*-position of similar constructs. Future work will investigate this aspect in 2PP additive manufacturing, allowing the production of artificial microniches and tissue-engineered constructs with stiffness gradients.

To explore whether the spatial *z*-position influences differentiation, hLESCs were seeded on two flat scaffolds with different heights, 20 µm (4.9 ± 2.5 kPa) and 200 µm (28.7 ± 7.2 kPa),

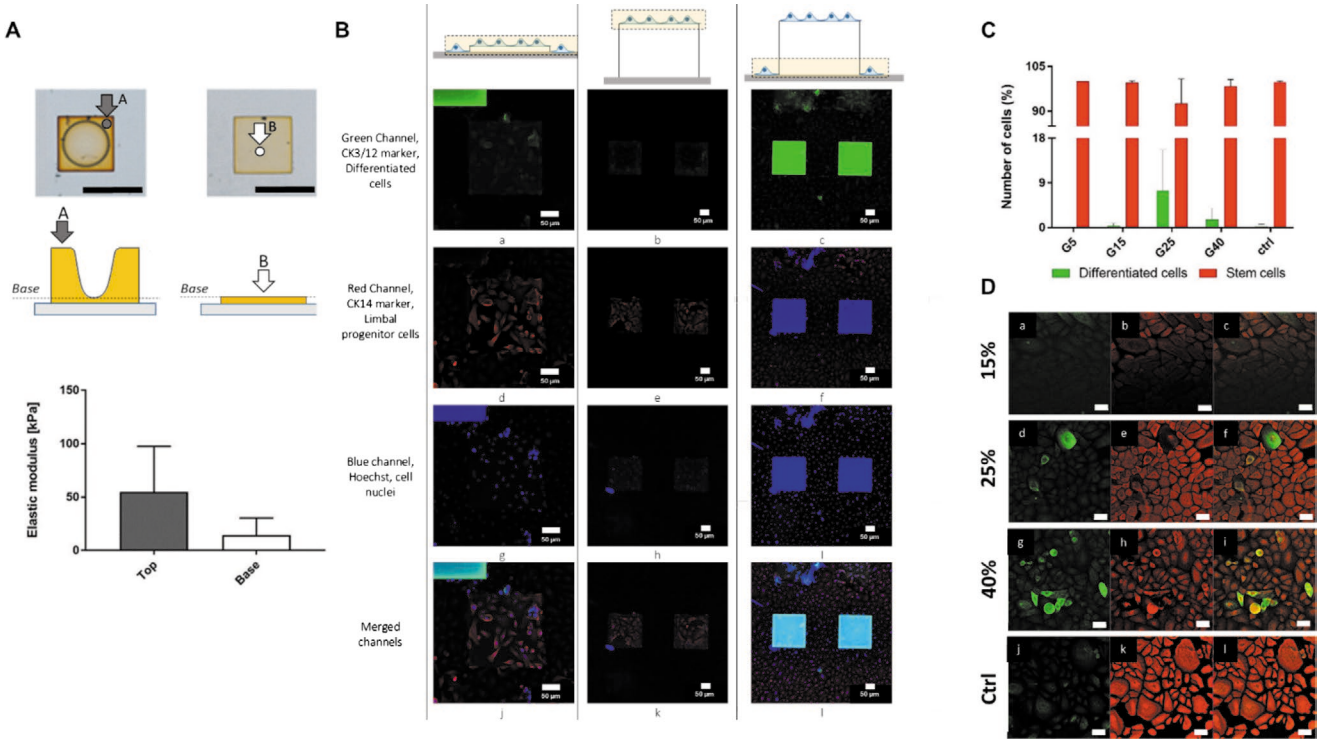

Figure 3. Surface elastic moduli of microniche structures according to *z*-position. A) Elastic moduli (kPa) of the rim (top; light grey) were different with the mean values of elastic moduli in the *z*-direction from three independent experiments indicating that the top was always stiffer although this was not statistically significantly different ($p = 0.09$, $n = 3$; error bars represent SD). Arrows indicate where measurements were taken. B) Confocal images of hLESCs on flat surfaces, stained with CK3/12 (green), CK14 (red), and Hoechst (blue). Cells were seeded on flat structures of a,d,g) 20 µm and b,e,h) 200 µm height, and on a glass c,f,i) surface. Green, red, blue, and merged channels are presented in the a–c) first, d–f) second, g–i) third row, and j–l) fourth row, respectively. Cells ($n = 3$) predominantly expressed the CK14 limbal progenitor cell marker (red) under all three conditions. The squares in the images indicate the location of the GelMA constructs. C) Number of stem cells and differentiated cells cultured on GelMA hydrogels of various stiffness (5, 15, 25, and 40% w/v). Percentages were calculated as the ratio of red-labeled (stem cells) and green-labeled cells (differentiated) to total cell numbers on three areas of each sample ($n = 2$; error bars represent ± SD, ANOVA, $p > 0.05$, post hoc with Bonferroni correction) in basal Cnt-Prime media. D) Confocal microscope images of hLESCs grown on GelMA hydrogels (15, 25, and 40% w/v) and cultured in CnT-PR basal media. Green (differentiated), red (progenitor cells), and merged images are represented in (a,d,g,j), (b,e,h,k), and (c,f,i,l) respectively (scale bar = 50 µm).

which were produced using the same printing parameters used for the base of the crypt structure. Since 2PP is a high-resolution printing method, whereby excitation is restricted to a tiny focal volume,[32] solidification of the photopolymer is strongly confined inside the focal volume throughout the multilayer processing procedure, and therefore the degree of polymerization is uniform throughout the printed microstructure (unpublished data). Results demonstrated that cells expressed the limbal progenitor cell marker (CK14) predominantly on both materials, independent of the differences in height and stiffness (Figure 3B).

There is some evidence that stiffness in the limbus may impact cell response.[31,33] However, Moers et al. have reported that stiffness impacted differentiation of corneal epithelial cells only on unphysiologically stiff substrates.[34] After 3 days of culture, corneal epithelial cells grown on physiologically relevant substrates (40 and 80 kPa) both maintained an early differentiation state, represented by the expression of cytokeratin 19. However, growth on unphysiologically stiff substrates (1.5 MPa) induced cell differentiation, denoted by the expression of the late differentiation marker cytokeratin 12.[34] To delineate the effects of stiffness versus spatial geometry of the fabricated microniches, hLESCs were seeded on flat GelMA substrates of varying stiffness. The average elastic moduli (±SD) for 15%, 25%, and 40% w/v GelMA substrates, obtained by compression testing, were 173.5 ± 78.2, 509.7 ± 60.4, and 1014.4 ± 75.5 kPa, respectively. Varying stiffness did not have a pronounced effect on stem cell differentiation. Numbers of stem cells and differentiated cells (Figure 3C,D) did not vary significantly (analysis of variance (ANOVA), $p > 0.05$, post hoc with Bonferroni correction) by increasing stiffness of flat substrates over the timeframe of the study in agreement with previous studies.[34] These results point to elimination of stiffness, within this range, as a contributor to cell fate and confirm that geometry is a major decisive factor for control of cell behavior.

To confirm the zonation in cell phenotype observed with commercial human primary stem cells (hLESCs), the same protocol was performed using freshly isolated cells from biopsy samples (td_hLESCs), supported by an underlying feeder layer of irradiated 3T3-J2 fibroblasts. Limbal epithelial cells were extracted from human cadaveric limbal biopsies and cultured using serum-supplemented media. CK3/12 was used as a differentiation marker and p63 as a stem cell marker (Figure S4, Supporting Information). Results revealed a zonation in marker

expression as was observed with commercially available cells, with cells at the base of the microniche expressing CK3/12 and cells at the rim expressing the stem cell marker p63.

We postulate that spatial geometry created a milieu of cellular signals inside the niche that enhanced cell differentiation at the base and not at the rim of the microniche construct, resulting in the observed cell differentiation gradient. A previous study reported that adipose-derived stem cell differentiation was localized within regions containing small, elongated cells (e.g., inner edge of a ring).[11] Therefore, the absence of complementary cues within the microniche in this study will have had an impact on the observed geometrically specific differentiation pattern. Maintenance of tissue homeostasis requires spatiotemporal cell organization to ensure tissue function.[35] While replicating the geometry and dimensions of the stem cell niche has a major influence over cell phenotype, as we report herein, cellular organization and phenotype within the niche is also influenced by other factors. Another potential parameter is the topography at the base. Previous studies have suggested that specific configurations, such as pillars (micropatterns of 11 vs 5 μm), can enhance the expression of late corneal keratinocyte markers.[34,36] Additionally, restricting the adhesive area of human epidermal stem cells triggered the initiation of terminal differentiation.[37] Further studies to understand the interplay between geometry and cell–cell signaling are needed to fully understand this phenomenon.

Mimicking intestinal crypt architecture using micromolded scaffolds has been previously reported, with a focus on recreating physiological chemical gradients using growth factors.[38] Few studies have specifically attempted to replicate limbal niche structures,[39,40] and have not replicated its precise dimensions.[19,20] Ortega et al., who reported that rabbit limbal cells populated ≈300 μm "micropockets," did not assess phenotypic expression[39] and have not used a clinically relevant cell type, which is vital since 3D morphology of limbal crypt structures varies between species.[41] In another study, the open ridge-like structures under investigation included stromal fibroblasts, and therefore the phenotypic response they reported in the limbal epithelial cell population cannot be attributed to geometry alone.[40] While limited investigation has been carried out into the importance of stem cell size and shape in 3D,[42] a geometrically induced, without the presence of a chemical gradient, differentiation gradient in a biologically relevant architecture has not been achieved, which is the significant finding in this study. This will have substantial impact on the design of in vitro stem cell niche models and novel "microniche-based" scaffolds for epithelial tissue regeneration.

In conclusion, we have demonstrated that mimicking the precise geometry of the epithelial stem cell niche impacts epithelial stem cell fate without the use of exogenous cues. This was achieved by producing microniches replicating in vivo architecture using 2PP, which allows the freedom to recreate structures at length scales appropriate for the production of stem cell microniches. The techniques described herein provide a tailorable platform for the development of synthetic microniches, allowing fine control over cell microenvironments. While this study provides the foundation for recreating epithelial stem cell crypts, further studies are necessary to build up the complexity of the constructed microniches and recreate cues from ECM and associated cells. It also provides a strategy to facilitate epithelial stem cell transplantation, whereby cells can be confined within implantable constructs that mimic characteristics of the stem cell microenvironment. This method is flexible and can be applied to other epithelial tissues, and as such represents a significant advance in the field of regenerative medicine.

Experimental Section

Chemicals were purchased from Sigma-Aldrich (UK) unless otherwise stated.

GelMA Synthesis: GelMA was synthesized as described previously.[43] Porcine skin gelatin (10% w/v type A, 300 bloom) was dissolved in phosphate-buffered saline (PBS; Gibco, UK) at 80 °C. Methacrylic anhydride (8% v/v) was added at 0.5 mL min^{-1} and stirred at 60 °C for 3 h. To quench the reaction, the solution was diluted 5× with PBS and stirred for a further 30 min. The solution was dialyzed against distilled water using 8 kDa cut-off dialysis tubing (BioDesignDialysis Tubing, USA) for 1 week at 50 °C. Dialysis water was changed three times per day. The solution was filtered through a 40 μm filter and lyophilized for 3 days. Freeze-dried GelMA was stored at –20 °C until use.

Quantification of Degree of Crosslinking: Percentage of methacrylation was quantified using ^{1}H NMR (400 MHz; Bruker UK Ltd., UK) at room temperature (RT). Phase and baseline corrections were applied before obtaining integrals of peaks of interest. MestReNova software (v6.0.2) was used to analyze spectra (64 scans). GelMA and gelatin were dissolved in deuterium oxide (10 mg mL^{-1}). Presence of a double bond signal (5.35–5.60 ppm) indicated addition of the methacrylate vinyl group. Percentage of methacrylation was calculated using the method described by Hoch et al.[44] The integral of the methylene peak (d = 2.7–2.9 ppm) was used for quantification of the lysine signal. Degree of substitution was determined by comparing lysine signals of modified and unmodified gelatin (Equation (1)). Intensity of the aromatic region (7–7.5 ppm) was used as reference

$$\text{Degree of methacrylation}\,(\%) = \left(1 - \frac{\text{lysine integration signal of GelMA}}{\text{lysine integration signal of gelatin}}\right) \times 100 \quad (1)$$

Degree of methacrylation was checked using the 2,4,6-TNBS assay. Gelatin and GelMA (4 mg) were dissolved in 0.25% v/v TNBS (in 0.01 M sodium hydrogen carbonate solution) and incubated at 40 °C for 3 h. Hydrochloric acid (3 mL 6N, Alfa Aesar, UK) was added and the solution was incubated at 80 °C for 1 h. After cooling, 4 mL deionized water was added and absorbance measured at 345 nm (Tecan Infinite M200 microplate reader). Degree of crosslinking was calculated according to Equation (2)

$$\text{Degree of methacrylation}\,(\%) = \left(1 - \frac{\text{Absorbance GelMA}}{\text{Absorbance gelatin}}\right) \quad (2)$$

2PP of GelMA to Create Crypt Structures: Polymeric solutions were prepared by mixing GelMA foam with the photoinitiator P2CK to obtain a suitable formulation. P2CK was prepared according a published protocol[45] or by a modified procedure. GelMA (15% w/v) was dissolved in PBS, and P2CK was added to a final concentration of 0.3% w/v. To fabricate microniches, a 2PP system (Nanoscribe Photonic Professional, GmbH, Germany) with a femtosecond laser emitting at 780 nm in galvo scan mode was used. The structure was developed using CAD 3D Autodesk Inventor software and printing parameters were set by the Describe software. The laser beam was focused using a conventional 63× microscope objective (Zeiss, NA 1.4 with oil immersion media) mounted on a linear stage for vertical positioning. The laser writing system was controlled by Nanowrite software. A drop of gel was cast between a 22 × 22 mm glass slide (thickness n.1.5), and an 18 × 18 mm

cover glass (thickness n.1.5), separated by a 300 μm spacer (Figure 1E). The printing process was achieved by tuning laser power, scan speed, and hatching distance. After printing, structures were "developed" by immersing samples in PBS (40 °C for 1 h) to remove nonpolymerized hydrogel; samples were then left at 4 °C overnight. Irgacure 2959 (0.1% w/v) was added and scaffolds were UV-cured (365 nm at 15 W) for 10 min to increase stability.

Determining Surface Elastic Modulus Using AFM: A thin cantilever (nominal spring constant between 0.07 and 0.025 N m^{-1}) with a silicon nitride tip (MSNL-10, probe A; Bruker Nano, UK) was used. The cantilever was positioned on the construct's rim and on a printed flat scaffold (height = 20 μm) to emulate the base of the scaffold. Force graphs were recorded using an MFP-1D AFM instrument (Asylum Research, USA) and elastic moduli (E) were calculated from the approaching force curves based on the Hertz model,[46] according to Equation (3)

$$E = \frac{3}{4}\frac{1-\mu^2}{\sqrt{R\delta^3}}F \tag{3}$$

where F is the applied force, R is the probe radius, δ is the indentation of the samples, E is the elastic modulus, and μ is the Poisson's ratio. Three experiments were conducted for each condition (A, B, and C). Numbers of modulus measurements in experiments A, B, and C were 278, 92, and 310 for the top and 158, 28, and 211 for the base, respectively.

Cell Culture of Xeno-Free Human Limbal Stem Cells: Commercial primary hLESCs were obtained from CELLnTEC Advanced Cell Systems (P2, single-donor; Switzerland) and cultured in serum-free epithelial culture media CnT-Prime (CnT-PR; CELLnTEC Advanced Cell Systems) with addition of 100 U mL^{-1} penicillin, 0.1 mg mL^{-1} streptomycin, and 0.25 μg mL^{-1} amphotericin B, and cultured at 37 °C and 5% CO_2. Cells were cultured at 4000 cells cm^{-2}.

Primary Cells Extracted from Human Corneal Biopsies: Td_hLESCs were collected from scleral-corneal tissue (obtained with written consent from next of kin according to the directives set by the Italian Centro Regionale Trapianti and Centro Nazionale Trapianti, and only when not suitable for transplantation) and preserved in media before processing. Biopsies, composed of cornea, limbus, and conjunctiva, were dissected into quarters, and then the cornea and conjunctiva were removed. The limbus was fragmented and soaked in PBS. Trypsin/EDTA (0.05%/0.01% w/v; Thermo Fisher Scientific, Italy) was added (10 mL) to digest the tissue for 30 min at 37 °C. The solution was centrifuged for 5 min at 1000 rpm and the pellet resuspended in fresh media. This cycle was repeated thrice to extract the majority of the cells. Cells were plated into a 24-well plate (30 000 cells per well) in coculture with irradiated 3T3-J2 cells. Culture medium consisted of Dulbecco's modified Eagle's medium (DMEM) and Ham's F12 (DMEM/F12, 2:1, Thermo Fisher Scientific) supplemented with 10% v/v FBS (Thermo Fisher Scientific), 50 μg mL^{-1} penicillin-streptomycin (P/S), 4×10^{-3} M glutamine (EuroClone, Italy), 5 μg mL^{-1} insulin (HUMULIN R, Lilly, Canada), 0.4 μg mL^{-1} hydrocortisone (Flebocortid Richter, Sanofi, Italy), 0.18×10^{-3} M adenine (adenine grade I, Pharma Waldhof GmbH, Germany), 8.1 μg mL^{-1} cholera toxin (Cholera Toxin QD, List Biological Laboratories, USA), 2×10^{-3} M triiodothyronine (Liotir, IBSA, Italy), and 10 ng mL^{-1} epidermal growth factor (GMP Cellgro, CellGenix GmbH, Germany).

Feeder Layer Preparation: Td_hLESCs were cultured on irradiated 3T3-J2 cells as a feeder layer. 3T3-J2 media consisted of DMEM supplemented with 10% v/v fetal calf serum (Thermo Fisher Scientific), 50 μg mL^{-1} P/S, and 4×10^{-3} M glutamine. Once confluent, cells were trypsinized and placed with a maximum of 20 mL culture media (1×10^6 cells mL^{-1}), then irradiated with a dose of 60 Grays (X-Ray Irradiator, CellRad, Faxitron). Cells were plated at 80 000 cells per well in 24-well plate.

Cell Seeding of the Microniche Constructs: hLESCs and td_LESCs suspensions (150 000 cells in 50 μL) were seeded onto the constructs. Afterwards, media was added to cover the entire surface of the scaffolds. For td_hLESCs, the feeder layer was seeded on the scaffold 4–24 h before adding keratinocytes. At 10 days post-seeding, cells were fixed for analysis.

Immunocytochemistry: Cells were dual-stained with either CK14 or p63 (limbal progenitor and stem cell markers, respectively) and CK3/12 (differentiated corneal epithelial cell marker). Following fixation, permeabilization was carried out using 0.1% v/v Triton X-100. Samples were exposed to blocking solution for 1 h (1% w/v bovine serum albumin (BSA; BDH Prolabo, USA) in PBS, 0.3 M glycine, and 3% v/v goat serum). Antibodies (Table S2, Supporting Information) were diluted in wash buffer (1% w/v BSA and 0.3 M glycine in PBS). Samples were incubated in primary antibodies overnight at 4 °C followed by secondary antibodies for 1 h at RT. Samples were washed and stained with Hoechst 33258. Fluorescent mounting medium (Dako, VWR, UK) was added prior to analysis by confocal microscopy (Zeiss Elyra PS1 microscope with ZEN software, Carl Zeiss, Germany).

Statistical Analysis: For the statistical analysis, GraphPad Prism 6 (v6.01) was used. For the AFM analysis, three experiments were conducted for each condition. Two-tailed Mann–Whitney U tests were performed to investigate differences in elastic moduli of the rim and base. In addition, mean AFM measurements of each sample were obtained and a two-sided paired t-test was performed ($n = 3$; error bars represent ±SD). All differences were considered statistically significant when $p \leq 0.05$. For the assessment of stem cell differentiation on GelMA constructs of different stiffness, a two-way ANOVA (area, two levels: top and bottom; GelMA concentration, five levels: 5, 15, 25, 40% w/v and control) with post hoc and Bonferroni correction was performed ($n = 2$; error bars represent ±SD). All differences were considered statistically significant when $p \leq 0.05$.

Supporting Information

Supporting Information is available from the Wiley Online Library or from the author.

Acknowledgements

This work was supported by the Engineering and Physical Sciences Research Council (EPSRC) and Medical Research Council (MRC) Centre for Doctoral Training in Regenerative Medicine (EP/L015072/1) doctoral training grant awarded to E.P. A short-term scientific mission awarded to E.P. was funded by the Biomedicine and Molecular Biosciences EU COST Action BM1302 "Joining Forces in Corneal Regeneration Research." 2PP fabrication was supported by the EPSRC Multifunctional Additive Manufacturing (EP/K005138/1), EPSRC Centre for Innovative Manufacturing in Additive Manufacturing (EP/I033335/2), and MRC UK Regenerative Medicine Platform Hub (MR/R015651/1). M.A. was supported by the EPSRC Programme Grant for Next Generation Biomaterials Discovery (EP/N006615/1). The authors acknowledge Robert Markus (University of Nottingham) for assistance with confocal microscopy (equipment funded by Biotechnology and Biological Sciences Research Council (BB/L013827/1)) and Xinyong Chen (University of Nottingham) for assistance with AFM.

Conflict of Interest

The authors declare no conflict of interest.

Author Contributions

E.P. and M.H.A. contributed equally to this work. The manuscript was written through contributions of all authors. E.P. carried out the experimental work and contributed to manuscript preparation. M.H.A. drafted the manuscript. Expertise in limbal stem cell isolation, culture, and characterization was provided by L.S., M.B., and S.F. Two-photon

amenable photoinitiators were synthesized by M.T., R.L., and J.M. Insights into corneal histology were provided by A.H. and H.D. The work was conceived, organized, and made possible with funding awarded to J.Y., R.W., and F.R.A.J.R. Manuscript drafting and submission was led by R.W. and F.R.A.J.R. All authors have given approval to the final version of the manuscript.

Keywords

cornea, differentiation, limbal stem cells, stem cell niche, two-photon polymerization

Received: January 20, 2020
Revised: March 22, 2020
Published online: April 24, 2020

[1] B. Ohlstein, T. Kai, E. Decotto, A. Spradling, *Curr. Opin. Cell Biol.* **2004**, *16*, 693.
[2] H. Yang, R. C. Adam, Y. Ge, Z. L. Hua, E. Fuchs, *Cell* **2017**, *169*, 483.
[3] F. M. WattB. L. M. Hogan, *Science* **2000**, *287*, 1427.
[4] M. F. Brizzi, G. Tarone, P. Defilippi, *Curr. Opin. Cell Biol.* **2012**, *24*, 645.
[5] S. Gobaa, S. Hoehnel, M. Roccio, A. Negro, S. Kobel, M. P. Lutolf, *Nat. Methods* **2011**, *8*, 949.
[6] F. Guilak, D. M. Cohen, B. T. Estes, J. M. Gimble, W. Liedtke, C. S. Chen, *Cell Stem Cell* **2009**, *5*, 17.
[7] S. Xiong, H. Gao, L. Qin, Y. G. Jia, L. Ren, *Bioact. Mater.* **2019**, *4*, 293.
[8] G. Q. Daley, *Cell Stem Cell* **2012**, *10*, 740.
[9] A. R. O'Callaghan, J. T. Daniels, *Stem Cells* **2011**, *29*, 1923.
[10] S. Masterton, M. Ahearne, *Exp. Eye Res.* **2018**, *177*, 122.
[11] L. Q. Wan, S. M. Kang, G. Eng, W. L. Grayson, X. L. Lu, B. Huo, J. Gimble, X. E. Guo, V. C. Mow, G. Vunjak-Novakovic, *Integr. Biol.* **2010**, *2*, 346.
[12] C. S. Chen, M. Mrksich, S. Huang, G. M. Whitesides, D. E. Ingber, *Science* **1997**, *276*, 1425.
[13] N. Jain, K. V. Iyer, A. Kumar, G. V. Shivashankar, *Proc. Natl. Acad. Sci. USA* **2013**, *110*, 11349.
[14] K. A. Kilian, B. Bugarija, B. T. Lahn, M. Mrksich, *Proc. Natl. Acad. Sci. USA* **2010**, *107*, 4872.
[15] M. Majdi, L. Wasielewski, A. R. Djalilian, in *Tissue-Specific Stem Cell Niche* (Ed: K. Turksen), Springer International Publishing, Cham **2015**, pp. 69–81.
[16] D. V. Patel, T. Sherwin, C. N. McGhee, *Invest. Ophthalmol. Vis. Sci.* **2006**, *47*, 2823.
[17] A. Miri, M. Al-Aqaba, A. M. Otri, U. Fares, D. G. Said, L. A. Faraj, H. S. Dua, *Br. J. Ophthalmol.* **2012**, *96*, 530.
[18] R. K. Molvaer, A. Andreasen, S. Heegaard, J. S. Thomsen, J. Hjortdal, S. F. Urbak, K. Nielsen, *Acta Ophthalmol.* **2013**, *91*, 457.
[19] H. S. Dua, V. A. Shanmuganathan, A. O. Powell-Richards, P. J. Tighe, A. Joseph, *Br. J. Ophthalmol.* **2005**, *89*, 529.
[20] V. A. Shanmuganathan, T. Foster, B. B. Kulkarni, A. Hopkinson, T. Gray, D. G. Powe, J. Lowe, H. S. Dua, *Br. J. Ophthalmol.* **2007**, *91*, 514.
[21] N. Di Girolamo, S. Bobba, V. Raviraj, N. C. Delic, I. Slapetova, P. R. Nicovich, G. M. Halliday, D. Wakefield, R. Whan, J. G. Lyons, *Stem Cells* **2015**, *33*, 157.
[22] H. S. Dua, J. S. Saini, A. Azuara-Blanco, P. Gupta, *Indian J. Ophthalmol.* **2000**, *48*, 83.
[23] U. Schlotzer-Schrehardt, T. Dietrich, K. Saito, L. Sorokin, T. Sasaki, M. Paulsson, F. E. Kruse, *Exp. Eye Res.* **2007**, *85*, 845.
[24] X. H. Qin, A. Ovsianikov, J. Stampfl, R. Liska, *BioNanoMaterials* **2014**, *15*, 49.
[25] Z. Chen, J. You, X. Liu, S. Cooper, C. Hodge, G. Sutton, J. M. Crook, G. G. Wallace, *Biomed. Mater.* **2018**, *13*, 032002.
[26] A. Richardson, E. P. Lobo, N. C. Delic, M. R. Myerscough, J. G. Lyons, D. Wakefield, N. Di Girolamo, *Stem Cell Rep.* **2017**, *9*, 1081.
[27] S. Pitz, R. Moll, *Prog. Retinal Eye Res.* **2002**, *21*, 241.
[28] C. Selhuber-Unkel, T. Erdmann, M. Lopez-Garcia, H. Kessler, U. S. Schwarz, J. P. Spatz, *Biophys. J.* **2010**, *98*, 543.
[29] J. A. Last, S. M. Thomasy, C. R. Croasdale, P. Russell, C. J. Murphy, *Micron* **2012**, *43*, 1293.
[30] P. Eberwein, J. Nohava, G. Schlunck, M. Swain, *Biophys. J.* **2014**, *106*, 789a.
[31] J. W. Foster, R. R. Jones, C. A. Bippes, R. M. Gouveia, C. J. Connon, *Exp. Eye Res.* **2014**, *127*, 37.
[32] C. Weingarten, S. Steenhusen, M. Hermans, E. Willenborg, J. H. Schleifenbaum, *Microfluid. Nanofluid.* **2017**, *21*, 165.
[33] R. R. Jones, I. W. Hamley, C. J. Connon, *Stem Cell Res.* **2012**, *8*, 403.
[34] K. Moers, T. Steinberg, G. Schlunck, T. Reinhard, P. Tomakidi, P. Eberwein, *Exp. Cell Res.* **2013**, *319*, 1889.
[35] A. X. da Silveira dos Santos, P. Liberali, *FEBS J.* **2019**, *286*, 1495.
[36] P. Eberwein, T. Steinberg, S. Schulz, D. Zimmermann, R. Accardi, D. Beck, T. Reinhard, P. Tomakidi, *Eur. J. Cell Biol.* **2011**, *90*, 1029.
[37] J. T. Connelly, J. E. Gautrot, B. Trappmann, D. W. M. Tan, G. Donati, W. T. S. Huck, F. M. Watt, *Nat. Cell Biol.* **2010**, *12*, 711.
[38] Y. Wang, R. Kim, D. B. Gunasekara, M. I. Reed, M. DiSalvo, D. L. Nguyen, S. J. Bultman, C. E. Sims, S. T. Magness, N. L. Allbritton, *Cell Mol. Gastroenterol. Hepatol.* **2018**, *5*, 113.
[39] I. Ortega, A. J. Ryan, P. Deshpande, S. MacNeil, F. Claeyssens, *Acta Biomater.* **2013**, *9*, 5511.
[40] H. J. Levis, R. A. Brown, J. T. Daniels, *Biomaterials* **2010**, *31*, 7726.
[41] K. Grieve, D. Ghoubay, C. Georgeon, O. Thouvenin, N. Bouheraoua, M. Paques, V. M. Borderie, *Exp. Eye Res.* **2015**, *140*, 75.
[42] M. Bao, J. Xie, A. Piruska, W. T. S. Huck, *Nat. Commun.* **2017**, *8*, 1962.
[43] J. W. Nichol, S. T. Koshy, H. Bae, C. M. Hwang, S. Yamanlar, A. Khademhosseini, *Biomaterials* **2010**, *31*, 5536.
[44] E. Hoch, C. Schuh, T. Hirth, G. E. Tovar, K. Borchers, *J. Mater. Sci. Mater. Med.* **2012**, *23*, 2607.
[45] Z. Q. Li, J. Torgersen, A. Ajami, S. Muhleder, X. H. Qin, W. Husinsky, W. Holnthoner, A. Ovsianikov, J. Stampfl, R. Liska, *RSC Adv.* **2013**, *3*, 15939.
[46] J. J. Roa, G. Oncins, J. Diaz, F. Sanz, M. Segarra, *Recent Pat. Nanotechnol.* **2011**, *5*, 27.